Material Science: An Indian Journal

Materials Science
ISSN: 0974-7486

Research | Vol 15 Iss 4

Green Synthesis of Zinc Oxide and Hydrogenated Zinc Oxide Catalysts

James D Onubun, Joshua L Konne* and Grace A Cookey

Department of Chemistry, Faculty of Science, Rivers State University, Nkpolu-Oroworukwo, Port Harcourt, Nigeria

***Corresponding author:** Joshua L Konne, Department of Chemistry, Faculty of Science, Rivers State University, Nkpolu-Oroworukwo, Port Harcourt, Nigeria, Tel: 234-81-3677-3590; E-mail: konne.joshua@ust.edu.ng

Received: October 30, 2017; **Accepted:** November 30, 2017; **Published:** December 8, 2017

Abstract

A novel green synthesis of zinc oxide catalysts using zinc nitrate, aqueous extract of plantain peel ash (for ZnO-PT control experiment) with hydrogen gas (for hydrogenated zinc oxide, ZnO-PTH) has been reported. The samples were characterized using XRD, SEM, EDS, UV and FT-IR. The XRD patterns of both samples showed characteristic reflections of ZnO with broader background for ZnO-PTH. Particle size estimations gave 50.67 and 52.93 nm for ZnO-PT and ZnO-PTH respectively. The SEM micrographs of ZnO-PH showed porous monophasic rod-like and rectangular polycrystallite plates while ZnO-PTH appeared largely biphasic (greyish and cloudy-patches) with larger pores. The EDS analysis showed Zn contents of both phases as approximately 50% and 56% in ZnO-PT and ZnO-PTH respectively. The UV-Vis of ZnO-PT nanoparticles in ethanol also showed different strong absorption bands at 310 nm, 330 nm and 360 nm while ZnO-PTH showed only at 320 nm in the UV region and two others at 580 nm and 620 nm in the visible region. Similarly, the FT-IR showed decrease in the wave number of bands (blue shift) for corresponding ZnO-PTH bands due to hydrogenation that caused ligand-metal charge transfer (LMCT). The results confirmed the formation of $Zn_{1-x}O$ (ZnO-PT) and ZnO_{1-x} (ZnO-PTH) phases respectively.

Keywords: ZnO-PT; ZnO-PTH; Plantain-peel-ash; Aqueous extract; Green-synthesis and Hydrogenated ZnO

Introduction

Zinc oxide (ZnO) is a white powdery inorganic compound that is nearly insoluble in water. It is widely applied as additive into numerous materials and products including ceramics, glass, cement, plastics, rubber (e.g. car tyres), lubricants, paints, ointments, adhesives, sealants, pigments, foods (source of Zn nutrient), fire retardants, batteries, ferrites, etc. In addition, ZnO is also a (II-VI) semiconductor with high exciton binding energy. It allows for excitonic transitions even at room temperature that provides applications in photoelectricity and laser emissions [1,2]. This is because of its band gap of 3.37 eV at room temperature and excitation binding of energy 60 MeV in the UV region. Thus, ZnO nanoparticles are efficient UV absorbers [3]. Structurally, ZnO crystallizes with a wurtzite structure that lacks centre of symmetry. This property combined with a large electromechanical coupling, results in strong piezoelectric and pyroelectric properties and hence the use of ZnO in mechanical actuators and piezoelectric sensors [2].

Citation: Onubun JD, Konne JL, Cookey GA. Green Synthesis of Zinc Oxide and Hydrogenated Zinc Oxide Catalysts. Mat Sci Ind J. 2017;15(4):122

Therefore, ZnO is an important semiconductor material due to these physico-chemical properties such as electrical, mechanical, optical, magnetic and chemical sensing properties [4]. Naturally, ZnO exist in the mineral called zincite. However, it is often synthesized for use depending upon its application demand. On the nanoscale, ZnO nanostructures have been shown to possessed catalytic properties due to their large surface area and high catalytic activity. Therefore, different synthetic techniques could enhance these properties. Hence, various methods for the synthesis of ZnO nanoparticles, like co-precipitation [5], chemical vapor synthesis [6], Solid-state reaction method [7], sputtering [8] andsol gel method [9,10] have been developed. However, most of these methods used inorganic hydroxides (e.g. NaOH) as precursor for their synthesis, which is expensive and toxic.

Till date, there is no information in literature on the use of extracts from natural waste materials as alkaline source for the synthesis of zinc oxide from zinc nitrate. Potassium has been identified as the most abundant element among others in plantain peels with an estimated value of 37 g kg^{-1} in the green peel [11,12]. This value increased by a small amount during the ripening process. However, plantain peels constitute significant percentage of domestic wastes in the Niger Delta being one of the predominant foods in the area [13].

Recently, hydrogenation of zinc oxide nanoparticles synthesized from sol-gel techniques with cassava starch as gelling agent has been reported [10]. The report showed that the hydrogenated zinc oxide (ZnO:H) phase was zinc rich (ZnO_{1-x}). This report will investigate the synthesis of Zinc oxide (ZnO-PT) and hydrogenated zinc oxide (ZnO-PTH) using aqueous extract of ash plantain peel (wastes) as the hydroxide (alkaline) source for both phases. This novel study would enhance waste to wealth generation for plantain peels.

Materials and Methods

Preparation of ZnO-PT and ZnO-PTH

Aqueous plantain peels ash solution: Fresh plantain peels were removed from 25 unripe plantains, washed, chopped into smaller pieces and oven-dried at 80°C. Thereafter, 110 g of the peels was ashed at 600°C for 5 h in a muffle furnace and cooled to room temperature. The resultant ash content obtained was 18.40 g (16.73%). This was dissolved in 200 ml of distilled water and filtered. The concentration of the filtrate was determined titrimetrically as 0.3 M alkaline solution using a 0.1 M solution of H_2SO_4 and methyl orange as indicator. The filtrate was warmed before reacting with a 200 ml of 0.15 M solution of zinc nitrate hexahydrate, $Zn(NO_3)^2.6H_2O$ in a 500 ml beaker to form white precipitates of zinc hydroxide. The use of warm filtrate was just to ensure quick reaction. Though the reaction also occur even with cold filtrate. The mixture was stirred and allowed to settle overnight under gravity. The supernatant was decanted and the precipitates dried overnight at 80°C to ensure the complete conversion of $Zn(OH_2)$ to ZnO (tagged ZnO-PT).

Synthesis of hydrogenated ZnO(ZnO-PTH)

ZnO-PTH was produced upon the reaction of ZnO-PT with hydrogen gas (generated from the reaction of some pieces of magnesium ribbon in a 50 ml of aqueous 6 M HCl). The reaction was carried out using a modified literature method of Konne and Christopher. The modification was in the use of a cocked Buchner flask in place of cocked conical flask. The Buchner flask allowed the direct passage of the liberated hydrogen gas into a glass tube containing ZnO-PT without the use

of a delivery or linkage glass tube. The ZnO-PT was heated mildly at 55°C during the reaction for 3 mins. The color of the ZnO-PT nanoparticles changed from white to light brown as the zinc rich phase (ZnO-PTH) emerged.

Characterization

The structural properties of the samples were analyzed using X-ray diffractometer, GBC Enhanced Mini-Material Analyzer. The samples were ground into powder and loaded on separate silicon wafers and slotted into the sample holders for XRD analysis. The 2θ angle range of 5°C-90°C was selected with a step size of 0.02. It is expected that characteristic peaks of ZnO appear within these angles. The average crystallite size (S) of the samples was estimated using Scherrer's formula (equation 1).

$$S = \frac{k\lambda}{\beta cos\theta} \qquad (1)$$

Where k is shape factor ~ 0.94, β is the full width at half-maximum and λ, the Cu anode Kα1 wavelength and θ is the Bragg's diffraction angle. It should be noted that the XRD results were received as image files from the centre where the samples were analyzed therefore re-plotting with excel software was not possible. However, previous reports on ZnO:H in literature was used to compare the peaks with the new results as repeated analysis was stalled due to the breakdown of the facility in the country [10].

The scanning electron microscope (SEM) equipped with an energy dispersive X-ray spectrometer (EDS) was used in characterizing the surface morphology and elemental constituents of the samples, respectively. The SEM samples were prepared with a little of the unground samples gummed on carbon sticky pads. These were placed on labeled aluminum stubs, screwed to sample holder and inserted into the SEM model ASPEX 3020 equipped with an Oxford EDS detector for analysis.

Similarly, the samples for UV-Vis analysis were dispersed in ethanol and scanned between 300 nm and 800 nm on a 2500 LaboMed spectrophotometer while using ethanol as the blank. Samples for FT-IR were ground with KBr and made into pellets for analysis on a PerkinElmer Spectrum 10.4.3 Infrared spectrophotometer. Each disc was placed in a sample holder positioned in the path of infrared radiation operating at a wavelength range of 350 nm-4000 nm before the analysis on a read out computer.

Results and Discussion

X-ray diffraction analysis

The X-Ray diffraction patterns of ZnO-PT and ZnO-PTH samples are shown in FIG. 1 (a) and 1 (b) respectively. The XRD peaks of both samples showed characteristic reflections of ZnO with minor (unknown/unlabeled) impurity peaks for ZnO-PTH. ZnO characteristic peak patterns begin with a triplet with the (101) reflection as the most intense. However, a lateral shift in Cu Kα1 and 2θ values was observed for both samples as compared to XRD data of the Joint Committee on Powder Diffraction Standards (JCPDS) card number, 00-005-0664 reported in literature [10,14,15]. This large difference in peak positions could be probably due to calibration or instrumental issues not doping. The particle size of the samples was estimated at 50.67 and 52.78 nm for ZnO-PT and ZnO-PTH respectively. Again, these results differ slightly from the broader background (consistent with smaller particle sizes and lower crystallinity) observed for ZnO-PTH (FIG. 1 (b)). The

reflections of ZnO-PT and ZnO-PTH (FIG. 1 (a)) showed that the samples were largely phase pure except a small peak due to the new phase in the case of ZnO-PTH. Previous studies have demonstrated that a new peak due to H-insertion emerged near the (110) peak position which matched with the labeled small ZnO:H peak as shown in FIG. 1 (b) [10]. The result also showed that the background of ZnO-PTH XRD pattern was noisier than that of ZnO-PT which might be due to the presence of the hydrogenated phase but needs further investigation. This assertion was supported by the SEM and FT-IR results.

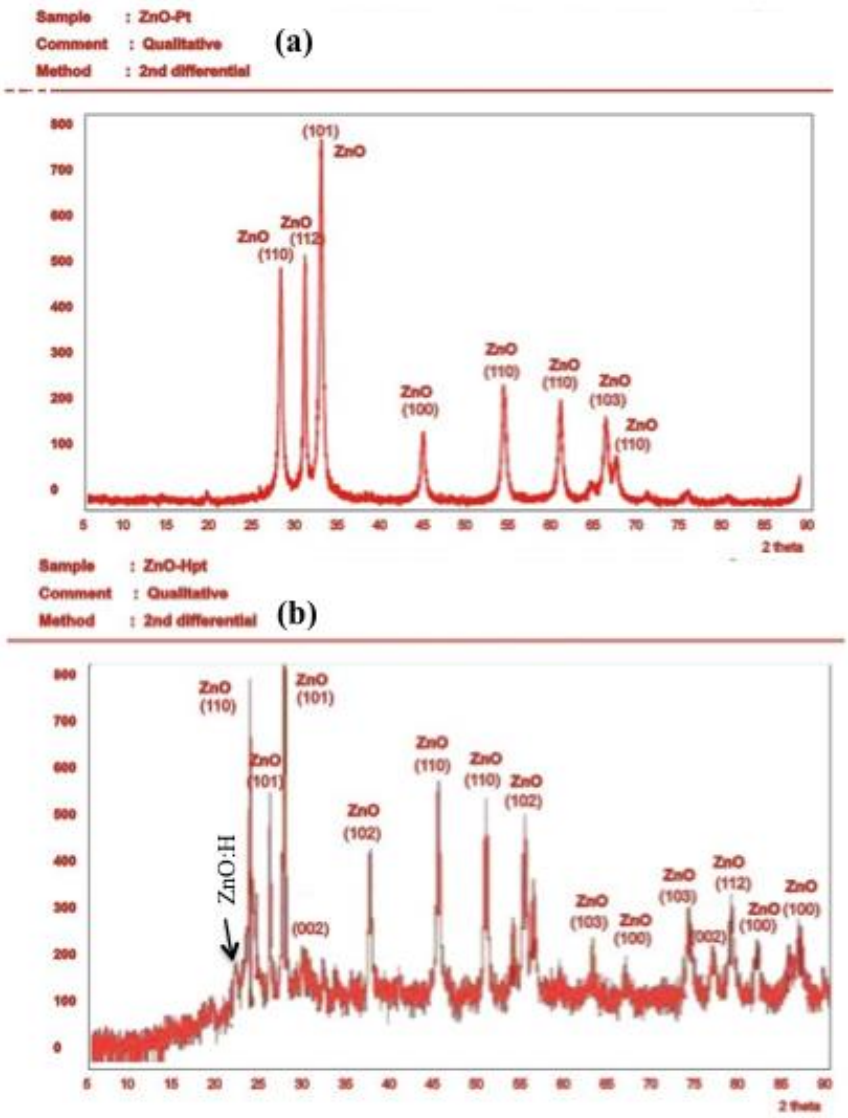

FIG. 1. **XRD reflections of (a) ZnO-PT and (b) ZnO-PTH.**

Morphological studies

The surface morphology of ZnO-PT and ZnO-PTH are shown in the SEM micrographs of FIG. 2 (a) and FIG. 2 (b) respectively. The former showed larger plate-like flowery polycrystallites than the later that was smaller and rod-like plates. Both structures appeared to be more compact than the images of the same samples (FIG. 2 (c) and 2 (d)) of ZnO-PT and ZnO-PTH, respectively that were used for EDS analysis. The image of the ZnO-PT sample (FIG. 2(c)), showed a uniform surface typical of a monophasic sample while ZnO-PTH was clearly biphasic with cloudy patches of hydrogenated phases.

ZnO-PTH polycrystallites were largely quasi-spherical in shape similar to Ag doped ZnO in literature [14]. The Zn contents of both samples were 50.88% and 55.70% for ZnO-PT and ZnO-PTH (FIG. 2 (c) and FIG. 2 (d)) respectively. This would be confirmed by other techniques in future work. Similar observations have been reported in previous work [10]. The higher Zn content of ZnO-PTH could be attributed to oxygen deficiency due to the presence of hydrogen while the ZnO-PT was almost 1:1 as expected. ZnO exists in two phases as ZnO_{1-x} and $Zn_{1-x}O$ depending on the prevailing oxygen conditions during synthesis and are known as native defects [16].

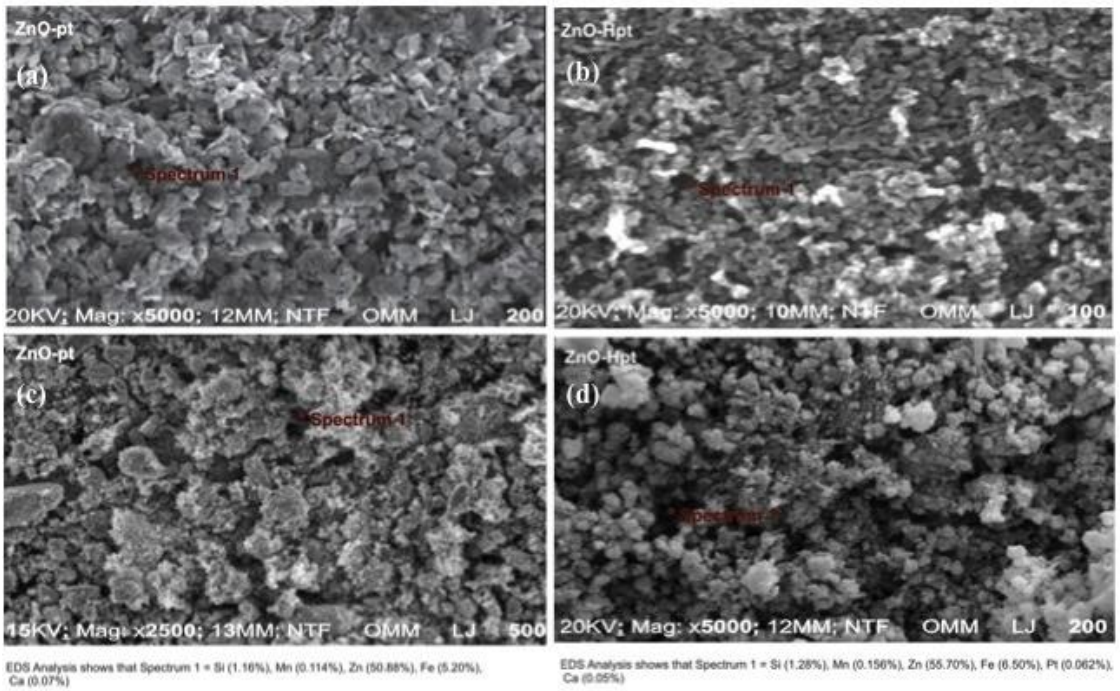

FIG. 2. **SEM and EDX of ZnO-PT (a and c) and ZnO-PTH (b and d) samples respectively.**

UV-Vis spectroscopy

The UV-Vis of ZnO-PT nanoparticles in ethanol scanned between 300 and 800 nm showed different strong absorption bands at 310 nm, 330 nm and 360 nm in the UV region while ZnO-PTH showed only one weak absorption band at 320 nm in the UV-Vis region and two others at 580 and 620 nm in the Vis region. This is shown in FIG. 3. The bands of excitation for the different wavelengths of ZnO-PT correspond to optical band gap of 3.97 ev, 3.75 ev and 3.43 ev, respectively. The hydrogenated zinc oxide (ZnO-PTH) shows weaker excitonic absorption peak at 320 nm in the UV-visible region which corresponds to optical band gap of 3.86 ev. However, the UV-Vis absorption pattern of ZnO-PTH was different from that reported for hydrogenated zinc oxide (ZnO:H) grown in starch solution where opposite absorption patterns were observed at 310 nm for both ZnO and ZnO:H respectively [10]. This may be connected with the higher Zn content (ZnO_{1-x} phase) observed against lower Zn content reported for ZnO:H in previous work but would need further investigation. The higher absorbance due to ligand-metal charge transfer (LMCT) band at 310 supports the fact that H substitutes oxygen vacancy to form a four-fold coordination with Zn in hydrogenated phases while zinc vacancy is substituted by two H-atoms [10]. Thus there would be more LMCT due to additional electrons from hydrogen in ZnO_{1-x} than in $Zn_{1-x}O$ phases, respectively leading to higher absorptivity in the former.

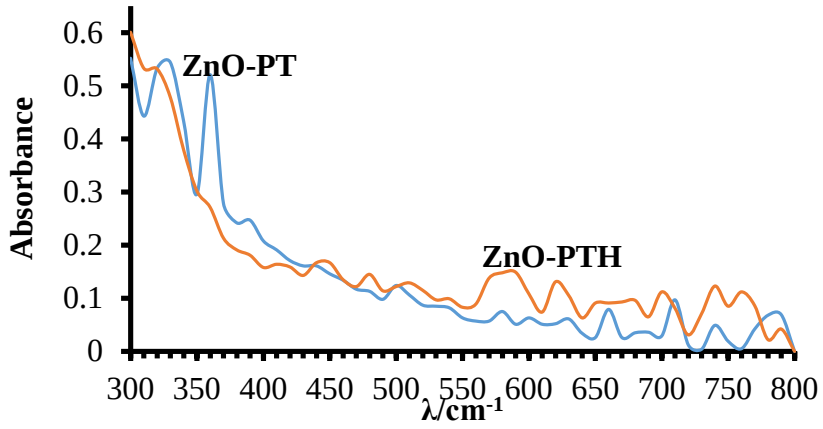

FIG. 3. **Uv-Vis of ZnO-PT and ZnO-PTH.**

FT-IR analysis

The FT-IR spectra of ZnO-PT and ZnO-PTH taken within 4000 cm^{-1}-400 cm^{-1} are shown in FIG. 4 while their labeled bands are listed in TABLE 1. The results showed slightly lower bands for some characteristic bands (360 cm^{-1}-1510 cm^{-1}) due to H-insertion in ZnO-PTH as compared to those of ZnO-PT. Additional electrons from H-atoms could cause the observed blue shift for ZnO-PTH bands. It was also observed that broad bands at 1766 cm^{-1}-2106 cm^{-1} in ZnO-PTH assigned to H-O stretching and deformation from absorbed water vapor in ZnO-PT (TABLE 1) was weaker after hydrogenation. This slight change in crystallinity might be responsible for the broad background observed on the XRD and also the biphasic morphology on the SEM of ZnO-PTH and is consistent with the FT-IR spectra of similar materials reported in literature [10]. The absorption band of metal oxides is generally in the fingerprint region below 1000 cm^{-1} which arises from inter-atomic vibrations.

TABLE 1. **Ft-Ir Of ZnO-PT And ZnO-PTH respectively obtained using Kbr pellet sample preparation.**

ZnO-PT	ZnO-PTH
362	361
467	378
713	463
833	713
949	833
1410	949
1377	1041
1462	1376
1507	1461
1462	1501
1766	2854
2106	2923
2854	3306
2923	

The peaks observed at (833 cm^{-1}-362 cm^{-1}) for ZnO-PT and ZnO-PTH respectively correspond to ZnO stretching and deformation vibrations. Other peaks observed at 2850 cm^{-1} and 2923 cm^{-1} were attributed to C-H stretching vibrations, 3242 cm^{-1} and 3306 cm^{-1} are those related to the presence of some hydroxyl groups while bands between 1410 cm^{-1} and 1507 cm^{-1} were assigned to C=O respectively [14]. ZnO could absorb water and CO_2 molecules from the atmosphere, hence the presence of such bands. The spectra (FIG. 4) also showed that ZnO-PT bands were more enhanced with an additional band compared to ZnO-PTH spectrum.

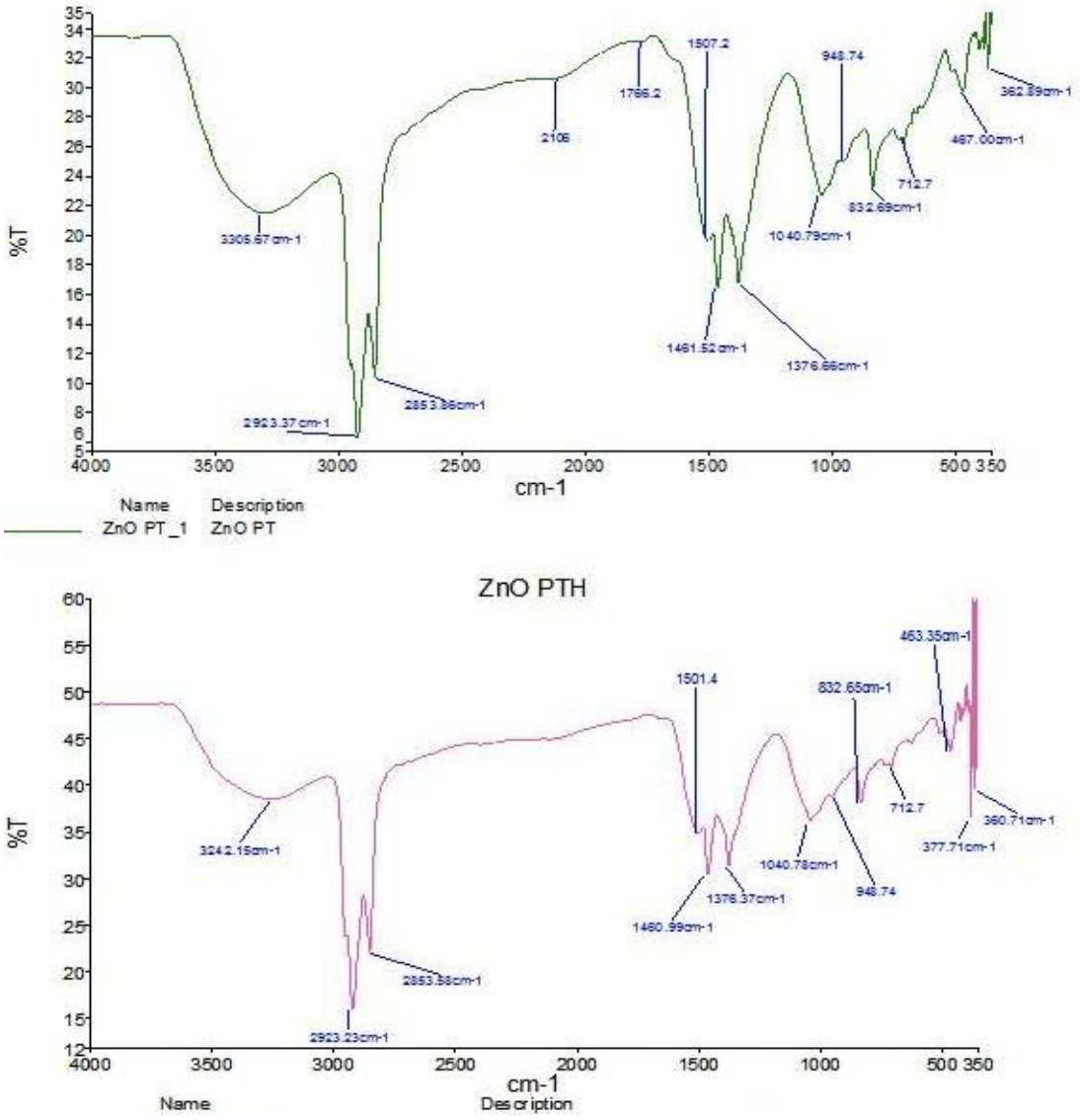

FIG. 4. **FT-IR spectra of ZnO-PT and ZnO-PTH respectively obtained using KBr pellet sample preparation.**

Conclusion

This report has demonstrated the successful synthesis of ZnO from the reaction of local materials (aqueous solution of plantain peels ash) with zinc nitrate hexahydrate. The ZnO nanoparticles were hydrogenated and characterized using XRD, SEM, EDS, UV and IR. The XRD patterns of both samples showed characteristic reflections of ZnO with minor

characteristic ZnO:H peak for ZnO-PTH. Particle size estimations gave 50.67 and 52.93 nm for ZnO-PT and ZnO-PTH respectively. The SEM micrographs of ZnO-PH showed porous monophasic rod-like and rectangular polycrystallite plates while ZnO-PTH appeared largely biphasic with larger pores. The EDS analysis showed Zn contents of both phases as approximately 50% and 56% in ZnO-PT and ZnO-PTH respectively and is recommended for confirmation in further studies. The UV-Vis of ZnO-PT nanoparticles in ethanol also showed different strong absorption bands at 310 nm, 330 nm and 360 nm while ZnO-PTH showed only at 320 nm in the UV region and two others at 580 nm and 620 nm in the visible region. Similarly, the FT-IR showed decrease in the wave number of bands (blue shift) for corresponding ZnO-PTH bands due to hydrogenation. The results confirmed that ZnO and ZnO-PTH (zinc rich phase) have been synthesized successfully using plantain peel extract as alkaline substitute for the commercial or toxic hydroxides.

Competing Interests

The authors declare that there are no competing interests regarding the publication of this article.

Acknowledgement

The authors would like to acknowledge Mr. D. Bekee of the Rivers State University for UV-visible analysis, Mr Collins Ofiwe of the Centre of Nanotechnology and Advanced Materials, Engineering Development Institute (EMDI), Akure, Ondo State, for the SEM, EDS and XRD analysis and Mr. Uwabueze Charles of the University of Ibadan for FT-IR analysis.

REFERENCES

1. Ko SC, Kim YC, Lee SS, et al. Micromachined piezoelectric membrane acoustic device. Sensors and Actuators A: Physical. 2003;103(1):130-4.
2. Zaouk D, Zaatar Y, Asmar R, et al. Piezoelectric zinc oxide by electrostatic spray pyrolysis. Microelectron J. 2006;37(11):1276-9.
3. Sudha M, Rajarajan M. Deactivation of photocatalytically active ZnO nanoparticle by surface capping with poly vinyl pyrrolidone. IOSR J Appl Chem. 2013;3:45-53.
4. Kolekar TV, Yadav HM, Bandgar SS, et al. Synthesis by sol-gel method and characterization of ZnO nanoparticles. ISRJ. 2011;1(1).
5. Kripal R, Gupta AK, Srivastava RK, et al. Photoconductivity and photoluminescence of ZnO nanoparticles synthesized *via* co-precipitation method. Spectrochimica Acta Part A: Spectrochim Acta A. 2011;79(5):1605-12.
6. Bacsa RR, Dexpert-Ghys J, Verelst M, et al. Synthesis and structure-property correlation in shape-controlled ZnO nanoparticles prepared by chemical vapor synthesis and their application in dye-sensitized solar cells. Adv Funct Mater. 2009;19(6):875-86.
7. Martin-González MS, García MA, Lorite I, et al. A solid-state electrochemical reaction as the origin of magnetism at oxide nanoparticle interfaces. J Electrochem Soc. 2010;157(3):E31-5.
8. Li LY, Cheng YH, Luo XG, et al. Room-temperature ferromagnetism and the scaling relation between magnetization and average granule size in nanocrystalline Zn/ZnO core-shell structures prepared by sputtering. Nanotechnology. 2010;21(14):145705.

9. You J, Chen CC, Dou L, et al. Metal oxide nanoparticles as an electron-transport layer in high-performance and stable inverted polymer solar cells. Adv Mater. 2012;24(38):5267-72.
10. Konne JL, Christopher BO. Sol-gel syntheses of zinc oxide and hydrogenated zinc oxide (ZnO: H) phases. Nanotechnology. 2017;2017.
11. Addison K. Making lye from wood ash [cited 2013 Jul 9]. Available from: http://journeytoforever.org/biodiesel_ashlye.html
12. T Happi, Emaga T, Andrianaivo RH, et al. Effects of the stage maturation and varieties on the chemical composition of banana and plantain peels. Food Chemistry. 2007; 103:590.
13. Izonfuo WAL, Omuaru VOT. Effect of ripening on the chemical composition of plantain peels and pulps. J Sci Food Agric. 1988;45:333.
14. Hosseini SM, Sarsari IA, Kameli P, et al. Effect of Ag doping on structural, optical and photocatalytic properties of ZnO nanoparticles. J Alloys Compd. 2015;640:408-15.
15. Swanson HE, Fuyat RK. Standard X-ray diffraction powder patterns. National Bureau of Standards (U.S.), Monograph 25, Circular, 539, 1. Available from: https://catalog.hathitrust.org/Record/001481228
16. Weller M, Overton T, Rourke J, et al. Inorganic Chemistry. 6th ed. Oxford, England, UK: Oxford University Press; 2002.